Available online at www.sciencedirect.com
ScienceDirect
Computerized Medical Imaging and Graphics 31 (2007) 418–427
Computerized Medical Imaging and Graphics
www.elsevier.com/locate/compmedimag

Computer vision guided virtual craniofacial reconstruction

Suchendra M. Bhandarkar [a], Ananda S. Chowdhury [a,*], Yarong Tang [a], Jack C. Yu [b], Ernest W. Tollner [c]

[a] *Department of Computer Science, The University of Georgia, Athens, GA 30602-7404, United States*
[b] *Department of Plastic Surgery, The Medical College of Georgia, Augusta, GA 30912-4080, United States*
[c] *Department of Biological & Agricultural Engineering, The University of Georgia, Athens, GA 30602-4435, United States*

Received 10 August 2006; received in revised form 15 March 2007; accepted 20 March 2007

Abstract

The problem of virtual craniofacial reconstruction from a sequence of computed tomography (CT) images is addressed and is modeled as a rigid surface registration problem. Two different classes of surface matching algorithms, namely the data aligned rigidity constrained exhaustive search (DARCES) algorithm and the iterative closest point (ICP) algorithm are first used in isolation. Since the human bone can be reasonably approximated as a rigid body, 3D rigid surface registration techniques such as the DARCES and ICP algorithms are deemed to be well suited for the purpose of aligning the fractured bone fragments. A synergistic combination of these two algorithms, termed as the hybrid DARCES–ICP algorithm, is proposed. The hybrid algorithm is shown to result in a more accurate mandibular reconstruction when compared to the individual algorithms used in isolation. The proposed scheme for virtual reconstructive surgery would prove to be of tremendous benefit to the operating surgeons as it would allow them to pre-visualize the reconstructed mandible (i.e., the end-product of their work), before performing the actual surgical procedure. Experimental results on both phantom and real (human) patient datasets are presented.

Keywords: DARCES; ICP; Bipartite graph matching; Computed tomography

1. Introduction

In fast-paced modern society, craniofacial fractures, especially mandibular fractures, are very frequently encountered with the prominent causes being gunshot wounds, motor vehicle accidents and sports-related injuries [1]. Frequently encountered craniofacial and mandibular fractures possess certain distinct patterns. Sometimes, these patterns imply a single fracture, and, in some other cases, a combination of single fractures [2]. From a surgical standpoint, the fractures are fixated one at a time in the operating room and hence must be so handled in the pre-surgical planning phase as well. Thus, practically speaking, in almost all the cases, reconstruction from a single mandibular fracture assumes paramount importance. The plastic surgeon in the operating room restores the form and function of the fractured bone elements in the craniofacial skeleton, typically, by first exposing all the bone fragments, then returning them to their normal configuration, and finally maintaining these reduced bone fragments with rigid screws and plates. However, there are several critical and inherent limitations to this current, standard approach. Complete visualization of the bone fragments in order to reduce them, necessitates their extensive exposure which consequently reduces the attached blood supply and impedes rapid healing. To improve the blood supply, the surgeon can decrease the extent of dissection and exposure. However, this implies that the surgeon is not able to visualize adequately the entire fracture, leading to potential misalignments of the bone fragments during reconstructive surgery. The proposed scheme for computer vision guided virtual craniofacial reconstruction from a sequence of computed tomography (CT) images allows the surgeon to reconstruct accurately the fractured craniofacial skeleton *in silico* before performing the actual surgery. Consequently, the surgeon is able to perform the actual surgery with minimum exposure of the bone fragments and with higher accuracy. The virtual craniofacial reconstruction scheme for single mandibular fractures, proposed in this paper can be used not only for pre-surgical planning but also as a training tool for surgery students and residents.

* Corresponding author. Tel.: +1 706 583 0613; fax: +1 706 542 2966.
E-mail addresses: suchi@cs.uga.edu (S.M. Bhandarkar), ananda@cs.uga.edu (A.S. Chowdhury), t3yr@yahoo.com (Y. Tang), jyu@mcg.edu (J.C. Yu), btollner@engr.uga.edu (E.W. Tollner).

0895-6111/$ – see front matter © 2007 Elsevier Ltd. All rights reserved.
doi:10.1016/j.compmedimag.2007.03.003

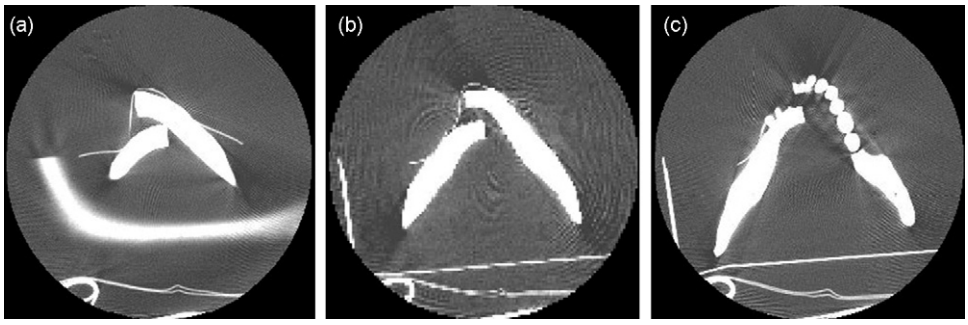

Fig. 1. A phantom CT image sequence of a fractured mandible. The image in (a) is a slice appearing at the beginning of the sequence, the image in (b) is a slice appearing at the middle of the sequence and the image in (c) is a slice appearing at the end of the sequence. These slices are not consecutive.

Much interesting research has been performed and reported, over the past decade, on various aspects of craniofacial and maxillofacial surgery. On account of space limitations, only a few representative works are mentioned here. The mass-tensor model is used for fast soft tissue prediction in [3] whereas the mass-spring model is used for fast surgical simulation from CT data in [4]. The iterative closest point (ICP) [5] algorithm is observed to be a popular computer vision algorithm for surface registration in the field of medical imaging [6]. The basic advantage of the ICP algorithm is that it yields an accurate result given a good initial starting point. Another surface registration algorithm called the data aligned rigidity constrained exhaustive search (DARCES) [7], which incorporates the well known random sample consensus (RANSAC) model fitting approach [8], is also popular because of its robustness to outliers and has been used extensively in medical imaging applications [9].

In this paper, we address the problem of virtual reconstruction of a single craniofacial (specifically, mandibular) fracture from a CT image sequence of the fractured bone fragments. Our principal contributions include: (a) exploration of the synergism between two philosophically different classes of surface reconstruction algorithms, namely the ICP and the DARCES algorithms, and (b) solution to the 3D correspondence problem within the ICP algorithm using a bipartite graph matching algorithm. A synergistic combination of the ICP and DARCES algorithms is observed to result in a greatly improved surface matching algorithm with significant reduction in the mean squared surface matching error (MSE). The work presented in this paper is a substantial extension of a preliminary version [10] wherein the experiments were limited to phantom data without any detailed analysis.

2. Image processing

The input to the computer vision guided virtual craniofacial reconstruction system is a sequence of 2D grayscale images of a fractured human mandible, generated using CT. Fig. 1 shows three non-consecutive CT image slices of a phantom mandible where the slice shown in Fig. 1a occurs at the beginning of the CT image sequence, the slice shown in Fig. 1b occurs in the middle of the CT image sequence and the slice shown in Fig. 1c occurs at the end of the CT image sequence. Fig. 2, on the other hand, is a CT image sequence obtained from a real (human) patient where the images shown in Fig. 2a–c represent three consecutive CT slices. A series of image processing tasks are undertaken before using the surface matching algorithms to register the two fractured bone fragments. The result of the image processing operations on the phantom CT slice in Fig. 1b is shown in Fig. 3 and on the real (human) patient CT slice in Fig. 2a is shown in Fig. 4. The software resulting from the implementation of the surface matching algorithms and image processing tasks is currently integrated into a JAVA-based package for computer-assisted reconstructive plastic surgery called *InSilicoSurgeon* (© The University of Georgia Research Foundation Inc., 2004). A brief description of the image processing tasks is as follows.

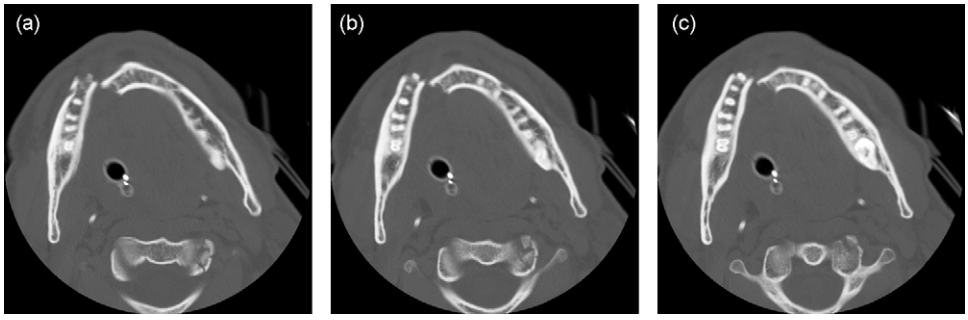

Fig. 2. A real patient CT image sequence of a fractured mandible. The images in (a)–(c) are three consecutive slices in the CT sequence.

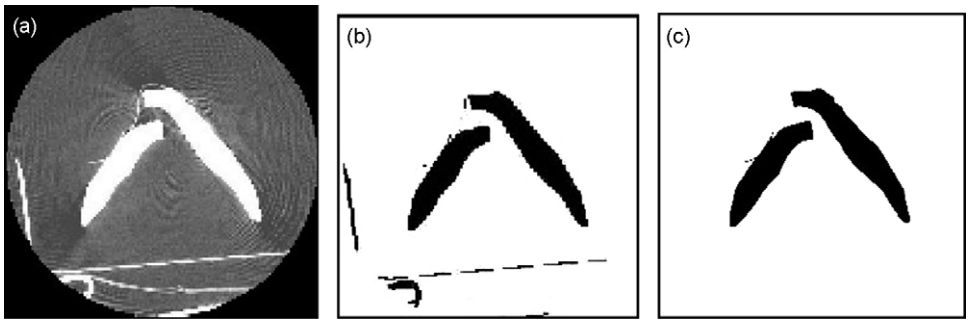

Fig. 3. (a) A typical 2D CT slice (from a phantom CT sequence). (b) The CT slice after simple thresholding. (c) The CT slice after connected component labeling and size filtering. In (b) and (c), the grayscale value 0 (i.e. color black) is used to represent mandible fragments and artifacts.

2.1. Thresholding

Two types of thresholding algorithms were used in the present work. For the phantom CT images, the bright components (having higher Hounsfield unit values [11]) represent the fractured mandible (bone) fragments whereas the dark areas (with relatively lower Hounsfield unit values) represent soft tissue. Hence, the threshold value for the binarization of the CT image was not difficult to select and simple thresholding was observed to be sufficient. Based on a priori knowledge, we classify a pixel with grayscale value above a certain threshold value T to belong to the object of interest and represent it using the grayscale value 0 (i.e., color black) as shown in Fig. 3b. Thus, for a grayscale CT image slice $G(i, j)$, we obtain a binary image $B(i, j)$ given by

$$B(i, j) = \begin{cases} 0 & \text{if } G(i, j) > T \\ 1 & \text{otherwise} \end{cases} \quad (1)$$

However, for real (human) patient CT data, the selection of the appropriate threshold is not obvious since the CT images typically contain objects or artifacts of different intensities (varying Hounsfield unit values). For example, a fractured mandibular fragment could contain cavities, dental fillings, crowns and other dental prostheses. In such cases, entropy-based thresholding [12] was found to perform better than simple thresholding. In the case of entropy-based thresholding, the threshold value (represented by the variable T) in Eq. (1) is determined via maximization of the inter-class entropy computed from the grayscale histogram of the CT image. The entropy, in general, is a probabilistic measure of the uncertainty of an event. For an image, the entropy S_c for each graylevel class c (consisting of several graylevel values) can be computed using the grayscale histogram as follows:

$$S_c = \sum_{k \in G_c} p(k) \log_2(p(k)) \quad (2)$$

where $p(k)$ is the probability of a pixel having a grayscale value k and G_c is the set of graylevels for class c. In the context of binarization, the graylevel threshold T is chosen such that the total entropy $S = \sum_{c=1}^{2} S_c$ is maximized.

2.2. Connected component labeling

Binarization of the CT image by itself cannot distinctly represent the two fracture fragments, as is evident from Figs. 3b and 4b. This is so because one still needs to filter out the undesired artifacts so that only the fractured mandibular fragments are used for the purpose of surface matching. A 2D connected component labeling (CCL) procedure in conjunction with a component area filter was used to remove the undesired artifacts (which are typically small in size). The threshold value for the component area filter was chosen to be 1000 pixels. Connected components with area less than the threshold value were deleted. The result of these operations is illustrated in Figs. 3c and 4c. The image processing tasks described thus far were performed on the individual 2D image slices comprising the CT image stack. The results of the 2D CCL were propagated across the CT image slices, resulting in a 3D CCL algorithm. A 3D component (a fractured jaw bone in this case) was identified by computing the area of overlap of the corresponding 2D components in successive CT image slices.

Fig. 4. (a) A typical 2D CT slice (from a real patient CT sequence). (b) The CT slice after entropy thresholding. (c) The CT slice after connected component labeling and size filtering. In (c), the two broken mandibular fragments are represented by two different intensity values.

2.3. Contour data extraction

After performing the thresholding, CCL and size filtering operations on all the CT image slices, the task of interactive contour detection was performed on the resulting binary image slices. We used two approaches for this purpose. In one approach, the user is required to click on the end points of the fracture contours in each of the binary image slices. The intervening contour points are automatically generated using a contour tracing algorithm. In the other approach, the user can click on potentially interesting points on a contour (typically points of high curvature). In both approaches, the contour points obtained from the individual binary image slices are collated to generate the 3D surface point dataset. A 3D surface point dataset is generated for each fracture surface.

3. Surface matching using the ICP algorithm

The task of the ICP algorithm [5] is twofold. The first task is to establish a correspondence between the two surface point sets to be matched. The second task is to compute the 3D transformation that brings the two sets into registration. In the present problem, the cardinalities of the two data sets to be matched are different. We denote the fracture surface (dataset) to be matched as the *sample* fracture surface (dataset) and the fracture surface (dataset) to which the sample fracture surface (dataset) is to be matched as the *model* fracture surface (dataset).

3.1. The basic ICP algorithm

The basic ICP algorithm consists of the following steps:

(1) The matching points in the model dataset corresponding to points in the sample dataset are determined. This new set of matching points in the model dataset, which represents a subset of the original model dataset, is termed the *closest* set.
(2) The 3D rigid body transformation (3D translation and 3D rotation) that brings the sample and model datasets into registration is computed. The transformation is obtained using the Theory of Quaternions [13].
(3) The computed transformation is applied to the original sample dataset and the mean squared error (MSE) between the transformed sample data points and the corresponding closest points is calculated. The MSE (ϵ^2) is given by

$$\epsilon^2 = \left(\frac{1}{n}\right)\sum_{i=1}^{n}(c_i - (Rs_i + T))^2 \tag{3}$$

where R denotes the rotation matrix, T denotes the translation vector, s_i denotes a point of the sample data set, c_i represents the corresponding point in the closest set and n is the total number of sample points.

Steps 1–3 are repeated with an updated sample dataset (generated by applying R and T obtained in the current iteration to the current sample dataset) until the difference in MSE between two successive iterations drops below a pre-specified threshold (0.01 mm^2 in our case).

3.2. Closest set computation

Graph theoretic matching has been used extensively in several computer vision problems [14]. In the computation of the closest set, which is the most crucial step in the ICP algorithm, the matching point pairs are determined using the maximum cardinality minimum weight (MCMW) bipartite graph matching algorithm based on the Hungarian method proposed by Kuhn [15]. We construct a bipartite graph $G(V_1 \cup V_2, E)$ where the 3D sample and model datasets correspond to the two disjoint vertex sets V_1, and V_2 respectively. The weight w_{ij} of an edge $e_{ij} \in E$ between two vertices v_i and v_j (where $v_i \in V_1$ and $v_j \in V_2$) is given by

$$w_{ij} = ((x_i - x_j)^2 + (y_i - y_j)^2 + (z_i - z_j)^2)^{1/2} \tag{4}$$

Theorem 1. *The worst-case time-complexity of the maximum cardinality minimum weight (MCMW) algorithm for a bipartite graph $G = (V_1 \cup V_2, E)$ with $|V_1| = |V_2| = n$ is $O(n^3)$.*

For the proof of the above theorem see [16].

Claim 1. *Given that there is neither a reflection nor a very large (e.g. greater than 90°) rotation (two extremely unlikely cases for a typical craniofacial injury), the maximum cardinality minimum weight (MCMW) algorithm for a bipartite graph correctly establishes the correspondence between two fracture surfaces at every stage of the iterative closest point (ICP) algorithm in polynomial time.*

Justification. Our justification is based on Theorem 1. Each fracture surface, consisting of several 3D data points, is modeled as a vertex set of a weighted bipartite graph $G = (V_1 \cup V_2, E)$. The bipartite graph is complete, i.e., there exists an edge $e_{ij} \in E$ between each vertex pair (v_i, v_j) where $v_i \in V_1$ and $v_j \in V_2$. The weight w_{ij} of edge e_{ij} is chosen to be the Euclidean distance between the corresponding vertices $v_i \in V_1$ and $v_j \in V_2$ where $i = 1, 2, \ldots n_1; n_1 = |V_1|$ and $j = 1, 2, \ldots n_2; n_2 = |V_2|$. The vertex set with lower cardinality is denoted as the *sample set* and that with the higher cardinality is denoted as the *model set*. The goal is to compute the *closest set*; i.e., a maximal subset of the model set wherein each point corresponds to a unique point in the sample set such that all points in the sample set are exhausted (principle of maximum cardinality) and simultaneously the sum of the edge weights between all pairs of corresponding points (i.e., $\sum w_{ij}$) is minimized (principle of minimum weight). This procedure is carried out in each iteration of the ICP algorithm. In absence of a reflection or a large (e.g. greater than 90°) rotation, this graph theoretic optimization procedure, with an objective function as the *sum of the Euclidean distances between all the pairs of matched points*, correctly matches a sample point with a model point without distorting the shape of the fracture surfaces. A greedy approach [17], based on the minimum Euclidean distance between individual pairs of points considered one at a time, on the other hand, would map more than

one sample point to a single model point and distort the fracture surface shape. Our problem formulation maps to the following well-known maximum cardinality minimum weight (MCMW) bipartite graph matching problem in graph theory, i.e., given a weighted complete bipartite graph $G = (V_1 \cup V_2, E)$ with edge-weights $w_{ij} \geq 0$; determine a pairing of the vertices from two vertex sets V_1 and V_2 such that the vertex set with smaller cardinality is completely exhausted and the total cost of the pairings is minimum. By virtue of its construction the proposed bipartite graph is complete with $E = V_1 \times V_2$ where $|V_1| \leq |V_2|$; such that $\exists$ 1:1 mapping $f : V_1 \rightarrow V_2$. From Theorem 1, the MCMW algorithm runs in $O(n^3)$ time for a bipartite graph with two vertex sets of equal cardinality n. In our case, $n = \max(n_1, n_2)$. Thus, the proposed solution clearly runs in polynomial time. □

4. Surface matching using the DARCES algorithm

The DARCES algorithm [7] is widely used for solving 3D registration problems efficiently and reliably, especially in the presence of outliers. The DARCES algorithm requires no local feature detection and no initial transformation estimation for the matching of two 3D data sets, and thus differs from most feature-based approaches or iterative approaches to the 3D registration problem.

4.1. The basic DARCES algorithm

The main steps in the DARCES algorithm are as follows:

(1) Reference points are selected from the sample data set. Note that the sample data set and the model data set have the same meaning as in the case of the ICP algorithm.
(2) From the set of reference points, three control points are chosen.
(3) Based on certain predefined geometric constraints, the three corresponding matching points in the model data set are determined. Note that for the three control points, there are many such sets of three matching points in the model data set.
(4) For each set of three pairs of corresponding points (i.e., the three control points and one set of three matched model points), a 3D rigid body transformation is obtained. Note that three pairs of corresponding points are sufficient to determine a 3D rigid body transformation.
(5) Each transformation is then applied to all the reference points other than the three control points. If the distance between a transformed point and its nearest model point is below a certain threshold, then this reference point is considered to have been successfully aligned to the model surface. Thus the number of successfully aligned sample data points is computed for each transformation.
(6) The transformation which has successfully aligned the maximum number of sample data points is deemed to be the solution to the registration problem.

5. Surface matching using the hybrid DARCES–ICP algorithm

Claim 2. *The hybrid DARCES–ICP algorithm is expected to yield a lower mean squared error (MSE) compared to that obtained by the DARCES and ICP algorithms in isolation.*

Justification. The DARCES algorithm helps in outlier rejection but the resulting transformation is only approximate. The ICP algorithm, on the other hand, yields a more accurate 3D rigid body transformation but is sensitive to outliers in the input data. Moreover, the pairs of matched points generated by the DARCES algorithm also helps in reducing the cardinalities of the two data sets to be matched (using bipartite graph matching [16]) in the ICP algorithm. Thus the relatively dense bipartite graph used to determine the closest set in the ICP algorithm can be reduced to a relatively sparse bipartite graph with fewer nodes and edges. The subsequent MCMW bipartite graph matching algorithm, (whose run time complexity is determined by the cardinalities of its vertex sets per Theorem 1) has a reduced computational complexity when run on a sparse bipartite graph. Simultaneously, a much lower MSE can be achieved for the matching of the two surfaces, since the DARCES algorithm provides a better starting point to the ICP algorithm by virtue of outlier removal. Thus, the synergistic combination of the DARCES and ICP algorithms, termed as hybrid DARCES–ICP algorithm (where the output of the DARCES algorithm is input to the ICP algorithm), is expected to yield a higher reconstruction accuracy. □

We have exploited the synergism between the DARCES and ICP algorithms in the following three different ways:

(1) Using the DARCES transformed sample dataset and the model dataset as the two inputs to the ICP algorithm. Thus, the initial transformation estimate of the ICP algorithm is the one resulting from the DARCES algorithm. This is termed as *Synergism 1*.
(2) Using a proper subset of the sample dataset (that has been aligned correctly by the DARCES algorithm) and the model dataset as the two inputs to the ICP algorithm. The initial transformation estimate used by the ICP algorithm is the default estimate, i.e., the initial rotation matrix is the identity matrix and the initial translation vector is the null vector. This is termed as *Synergism 2*.
(3) Using the DARCES transformed subset of the sample dataset and the model dataset as the two inputs to the ICP algorithm. Here, the proper subset of the sample dataset that has been aligned correctly by the DARCES algorithm is used. Also, the initial transformation estimate of the ICP algorithm is the one resulting from the DARCES algorithm. This is tantamount to the combination of *Synergism 1* and *Synergism 2* and is termed as *Synergism 3*.

The composite transformation matrix $\theta_{\text{DARCES–ICP}}$ of the hybrid DARCES–ICP algorithm (consisting of a rotation matrix

and a translation vector), to be applied to the sample dataset in order to register it with the model dataset is given by

$$[\theta_{\text{DARCES–ICP}}] = [\theta_{\text{DARCES}}]\,[\theta_{\text{ICP}}] \quad (5)$$

where θ_{DARCES} and θ_{ICP}, respectively denote the composite transformations obtained from the individual DARCES and ICP algorithms.

6. Experimental results

Table 1 compares the reconstruction accuracy of the ICP, the DARCES and the hybrid DARCES–ICP algorithms for a typical phantom and a typical real (human) patient dataset. In both the cases, the hybrid DARCES–ICP algorithm outperforms the individual ICP and DARCES algorithms. The convergence in the case of the hybrid DARCES–ICP algorithm is achieved within three to four iterations as compared to six to eight iterations for the original ICP algorithm. However, in the case where each fracture surface dataset consists of only the interest points (essentially points of high curvature), both the DARCES and the ICP algorithms take only a few seconds more than the hybrid DARCES–ICP algorithm for completion. For example, in the case of real (human) patient CT data, all the three algorithms finished their execution within well less than a minute on a 1.73 GHz *Intel© Pentium© M* Processor. Although the hybrid DARCES–ICP algorithm is observed to result in lower surface matching error, its computational benefit (in terms of execution time) compared to that of the ICP algorithm used in isolation is perceivable only in cases where the input datasets to the ICP algorithm are very dense. In such cases, the DARCES component of the hybrid DARCES–ICP algorithm can be used to greatly prune the sample dataset by virtue of outlier removal. Subsequently, the ICP component of the hybrid DARCES–ICP algorithm would run with a considerably sparse sample dataset, resulting in a perceivably lower computation time.

Table 2 shows the impact of the various levels of synergism between the ICP and DARCES algorithms (discussed in Section 6) on the MSE. It is interesting to note that not all the ways of exploiting synergism between the DARCES and ICP algorithms are equally effective. The subset of the sample dataset that is properly aligned by the DARCES algorithm consists of the original sample dataset with possible outliers removed. When the ICP algorithm is run on this filtered dataset, with the initial transformation estimate as the output of the DARCES algorithm (i.e., Synergism 3), the lowest MSE is achieved.

Table 1
A comparison of mean squared error values for the three different reconstruction algorithms for one set of phantom and one set of real patient data

Type of data	Reconstruction algorithm	Mean squared error (mm^2)
Phantom	DARCES	0.33
Phantom	ICP	0.91
Phantom	Hybrid DARCES–ICP	0.25
Real patient	DARCES	4.02
Real patient	ICP	2.07
Real patient	Hybrid DARCES–ICP	1.24

Table 2
A comparison of the mean squared error values of the hybrid DARCES–ICP algorithm, resulting from extraction of synergism between the DARCES and the ICP algorithm in three different ways

The way synergism is exploited between the DARCES and the ICP algorithms	Mean squared error of the hybrid DARCES–ICP algorithm (mm^2)
Synergism 1	2.07
Synergism 2	1.65
Synergism 3	1.24

Figs. 5 and 6, respectively show the original as well as the reconstructed CT image subsequence obtained using the ICP, DARCES and hybrid DARCES–ICP algorithms for a phantom dataset and a real (human) patient dataset. It is quite difficult to visually compare the reconstruction results since the MSE values are of the order of a few mm. Thus, the numerical results in Tables 1 and 2 are the best measure by which to evaluate the performance of the various reconstruction algorithms.

Fig. 7 displays the rendered volume of the fractured and the reconstructed mandible using the hybrid DARCES–ICP algorithm for a CT image dataset of a real (human) patient. The rendering has been performed using the VolumeJ [18] plugin in the ImageJ software package. We have used the *raytrace rendering algorithm* with *trilinear interpolation* and *gradient no index* classifier options.

The experiments were carried out using the software package InSilicoSurgeon, which was developed by us and is currently built on top of ImageJ, the imaging software from NIH [19]. Our software contains a simple but elegant graphical user interface (GUI) which can be used to great advantage for the purpose of virtual surgery and pre-surgical planning as well as surgical training. This GUI is shown in Fig. 8. The interface has three broad sections, namely (a) *image processing*, (b) *r* econstruction algorithms and (c) *miscellaneous*. Each section in turn consists of three buttons. All the buttons perform a dedicated task which is evident from their names. For example, the user can click on the CCL button to perform the connected component labeling, click on the *display registered* button to bring the fractured bone fragments into registration (using any of the three reconstruction algorithms), click on the *erase artifact* button to manually remove any undesired artifact (an interactive facility) and so on. Additionally, a *help* button is provided for general assistance and guidance.

7. Conclusions and future work

Two philosophically different classes of surface matching algorithms namely the ICP and the DARCES algorithms were employed for computer vision guided virtual craniofacial (specifically mandibular) reconstruction. The correspondence problem within the ICP algorithm was solved in a novel manner using the MCMW bipartite graph matching algorithm. A novel synergistic combination of these two algorithms, termed as the hybrid DARCES–ICP algorithm, was proposed. The hybrid DARCES–ICP algorithm was observed to yield the highest reconstruction accuracy on both the phantom as well as real

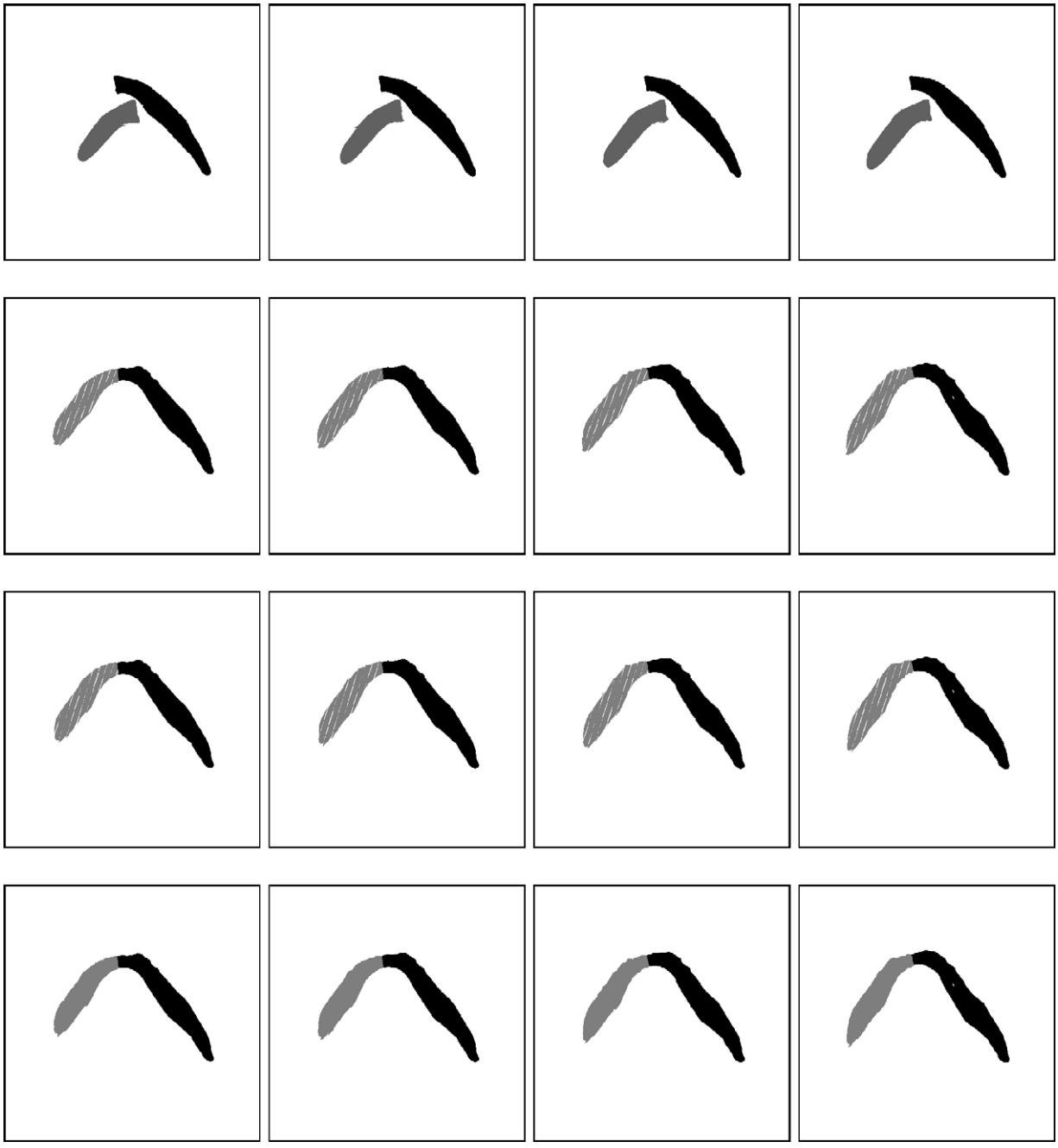

Fig. 5. The first row represents broken mandible fragments in phantom CT slices. The second, third and fourth rows, respectively represent reconstruction resulting from DARCES, ICP and hybrid DARCES–ICP algorithms.

(human) patient datasets. A simple yet elegant graphical user interface (GUI) was developed for the surgeons to execute various image processing (thresholding, CCL) and computer vision (the three surface matching algorithms)-based tasks.

Future research would focus on (a) the development of an objective function, consisting of shape symmetry and biomechanical stability in addition to the surface matching error, which could then be used as a measure of reconstruction performance, (b) automation of the fracture surface data extraction process, and (c) ensuring correct correspondence between the fracture surface datasets in the case of significant rotation and reflection by imposing geometrical constraints (in addition to those incorporated within the bipartite graph matching algorithm).

8. Summary

The work presented in this paper addresses the problem of computer vision-assisted virtual craniofacial (specifically mandibular) reconstruction from two fractured fragments. Two different surface matching algorithms namely the data aligned rigidity constrained exhaustive search (DARCES) and the iterative closest point (ICP) are employed individually for this

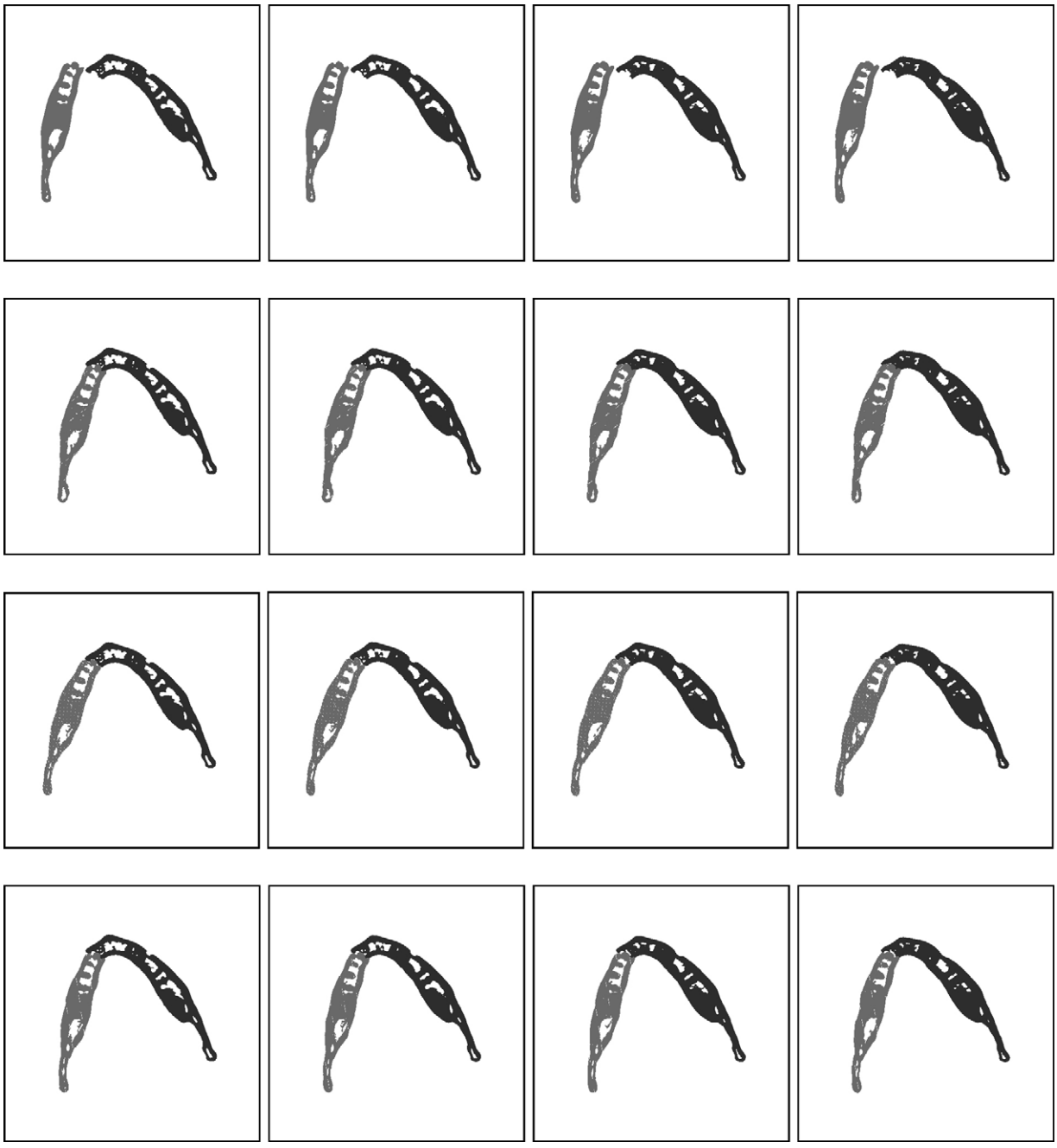

Fig. 6. The first row represents broken mandible fragments in real patient CT slices. The second, third and fourth rows, respectively represent reconstruction resulting from DARCES, ICP and hybrid DARCES–ICP algorithms.

purpose. An innovative graph theoretic approach is taken to solve the correspondence problem in the ICP algorithm.

The synergism between the DARCES and ICP algorithms is exploited in different ways with different degrees of impact on the final reconstruction accuracy. A simple but elegant graphical user interface is developed to help the surgeon perform necessary image processing (thresholding, connected component labeling) and computer vision (surface reconstruction using DARCES, ICP and hybrid DARCES–ICP algorithms) tasks as part of virtual surgical reconstruction. Experimental results on both phantom and real (human) patient CT data are presented.

Acknowledgments

The research was supported in part by a research grant from the University of Georgia–Medical College of Georgia Joint Research Program administered by the Biomedical and Health Sciences Institute at the University of Georgia and by an Engineering Research Grant by the Faculty of Engineering at the University of Georgia. The authors sincerely acknowledge the help of Professor Robert W. Robinson, Department of Computer Science, The University of Georgia for fruitful discussions on the bipartite graph matching algorithm and Dr. Ramon Figueroa,

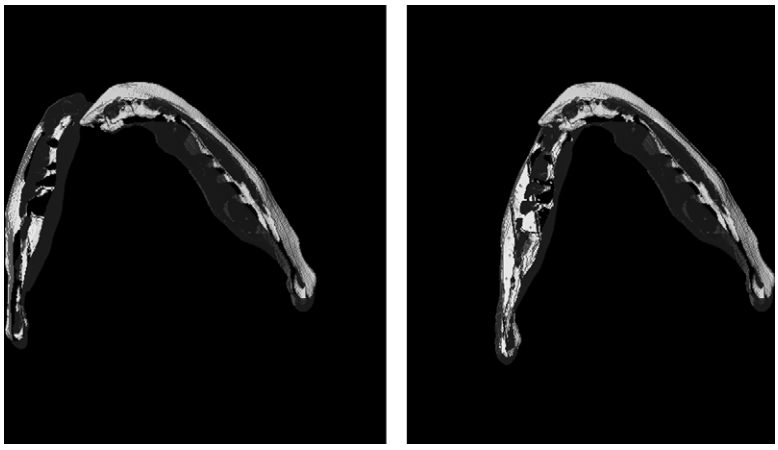

Fig. 7. A Visual comparison of the rendered volume of the broken jaw and the reconstructed jaw (using the hybrid DARCES–ICP algorithm).

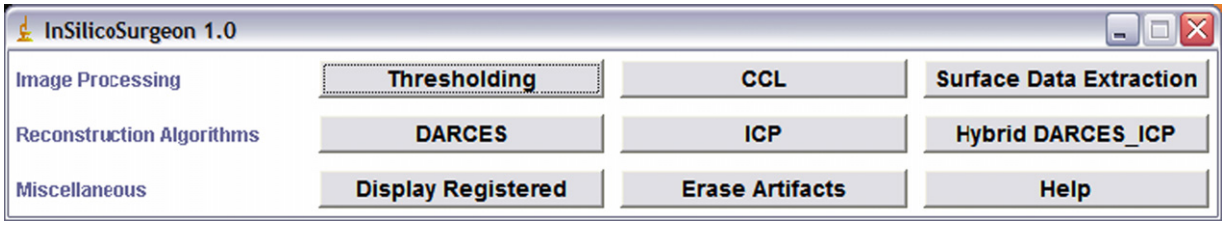

Fig. 8. A snapshot of the graphical user interface (GUI) for the virtual surgical reconstruction.

Department of Radiology, Medical College of Georgia for providing the CT scans. The authors also thank the anonymous reviewers for their insightful comments which greatly improved the paper.

References

[1] King RE, Scianna JM, Petruzzelli GJ. Mandible fracture patterns: a suburban trauma center experience. Am J Otolaryngol 2004;25(5):301–7.
[2] Ogundare BO, Bonnick A, Bayley N. Pattern of mandibular fractures in an urban major trauma center. J Oral Maxillofac Surg 2003;61(6):713–8.
[3] Mollemans W, Schutyser F, Nadjmi N, Suetens P. Very fast soft tissue predictions with mass tensor model for maxillofacial surgery planning systems. In: Proceedings of the 9th annual conference of the international society for computer aided surgery; 2005. p. 491–96.
[4] Keeve E, Girod S, Girod B. Craniofacial surgery simulation. In: Proceedings of the fourth international conference on visualization in biomedical computing (VBC). Hamburg, Germany; 1996. p. 541–46.
[5] Besl PJ, McKay ND. A method for registration of 3-D shapes. IEEE Trans Pattern Anal Mach Intell 1992;14(2):239–56.
[6] Granger S, Pennec X, Roche A. Rigid point-surface registration using an EM variant of ICP for computer guided oral implantology, In: Proceedings of the fourth international conference on medical image computing and computer assisted intervention (MICCAI). Utrecht, The Netherlands; 2001. p. 752–61 [LNCS 2208].
[7] Chen CS. RANSAC-based DARCES: a new approach to fast automatic registration of partially overlapping range images. IEEE Trans Pattern Anal Mach Intell 1999;21(11):1229–34.
[8] Fischler MA, Bolles RC. Random sample consensus: a paradigm for model fitting with applications to image analysis and automated cartography. Commun ACM 1981;24:381–95.
[9] Rogers M, Graham J. Robust active shape model search for medical image analysis. In: Proceedings of the seventh international conference on medical image understanding and analysis (MIUA). Portsmouth, UK; 2002. p. 21.
[10] Bhandarkar SM, Chowdhury AS, Tang Y, Yu JC, Tollner EW. Surface matching algorithms for computer aided reconstructive plastic surgery. In: Proceedings of the second IEEE international symposium on biomedical imaging (ISBI); 2004. p. 740–43.
[11] Hounsfield GN. Nobel award address: computed medical imaging. Med Phys 1980;7(4):283–90.
[12] Sahoo PK, Soltani S, Wong KC, Chen YC. A survey of thresholding techniques. Comput Vis Graph Image Process 1988;41:233–60.
[13] Hamilton WR. On quaternions. Proc R Ir Acad 1847;3:1–16.
[14] Kim W, Kak AC. 3-D object recognition using bipartite matching embedded in discrete relaxation. IEEE Trans Pattern Anal Mach Intell 1991;13(3):224–51.
[15] Kuhn HW. The Hungarian method for the assignment problem. Nav Res Log Quart 1955:2.
[16] Christofides N. Graph theory: an algorithmic approach. Academic Press; 1975.
[17] Cormen TH, Leiserson CE, Rivest RL, Stein C. Introduction to algorithms. MIT Press; 2001.
[18] Abramoff MD, Viergever MA. Computation and visualization of three dimensional motion in the orbit. IEEE Trans Med Imag 2002;21(4):296–304.
[19] Rasband WS. ImageJ, Bethesda, MD, USA: U.S. National Institutes of Health. http://rsb.info.nih.gov/ij/; 1997–2006.

Suchendra M. Bhandarkar received a B.Tech. in Electrical Engineering from the Indian Institute of Technology, Bombay, India in 1983, and an M.S. and Ph.D. in Computer Engineering from Syracuse University, New York in 1985 and 1989, respectively. He is currently a professor in the Department of Computer Science at the University of Georgia, Athens, Georgia where he directs the Visual and Parallel Computing Laboratory (VPCL). Dr. Bhandarkar was a Syracuse University Fellow for the academic years 1986–1987 and 1987–1988. He is a member of the IEEE, AAAI, ACM and SPIE. He is a coauthor of the book "Object Recognition from Range Images" (Springer Verlag, 1992). He is also a member of the honor societies Phi Kappa Phi and Phi Beta Delta. His research interests include computer vision, pattern recognition, multimedia systems, artificial intelligence and parallel algorithms and architectures for

computer vision and multimedia. He has over 100 published research articles in these areas including over 50 articles in peer-reviewed archival journals. Dr. Bhandarkar serves on the editorial boards of the Computer Journal, Applied Intelligence Journal and the Machine Vision and Applications Journal and on the program committees of several international conferences and symposia. He serves on advisory panels of government agencies such as NASA, Department of Defense, Department of Energy and Department of Health and Human Services.

Ananda S. Chowdhury received a B.Sc. (with Hons.) in Physics from Presidency College, Calcutta, India in 1996, followed by a B.Tech. in Electronics Engineering from the Institute of Radiophysics and Electronics, Calcutta, India in 1999, and an M.E. in Computer Engineering from Jadavpur University, Calcutta, India in 2001. After a one-and-half year (from June 2001 to December 2002) brief stint in industry as a software engineer, he is currently pursuing the Ph.D. degree in Computer Science at the University of Georgia, Athens, Georgia starting from 2003. His research interests include computer vision, pattern recognition and image processing. He is a student member of the IEEE and IEEE Computer Society.

Yarong Tang graduated from University of Georgia in 2003, with an M.S. degree in Artificial Intelligence. She is currently in the masters program in Biometry at Lousiana State University Health Sciences Center at New Orleans.

Jack C. Yu is professor and chief of Plastic Surgery and chief of Pediatric Plastic Surgery as well as the director of the MCG Craniofacial Center at the MCG Children's Medical Center and currently heads the monthly Cleft Lip and Palate and the Craniofacial programs at MCG. He completed medical school at the University of Pennsylvania. He completed his residency in general surgery and plastic surgery at the Hospital of the University of Pennsylvania. Dr. Yu also completed his craniofacial surgery fellowship at the Hospital of the University of Pennsylvania and Children's Hospital of Philadelphia. Dr. Yu is board certified by the National Board of Dental Examiner, Northeast Regional Board in Dentistry, American Board of Surgery and the American Board of Plastic Surgery. He is currently on the Biomaterials and Research Committee for the American Society of Maxillofacial Surgeons, Member of the Advisory Council for Mathematical Sciences for the State of Georgia, Continuing Education Committee for the American Cleft Palate–Craniofacial Association, and Development Committee for the Plastic Surgery Research Council, and International Society of Craniofacial Surgeons. His clinical interests focus on deformities of the craniofacial region in both adults and children, as well as cosmetic surgeries of the face.

Ernest W. Tollner is a native of Maysville, KY and received his B.S. and M.S. degrees in agricultural engineering at the University of Kentucky. He did his doctorate at Auburn. His graduate work was concerned with computer modeling erosion control, water resource development and animal waste management. This work provided the foundation for extension into composting, bioconversion and imaging research. Tollner was among the first to use topographic scanning for charactering soils, food products and logs. Research over the past 25 years at the University of Georgia has resulted in over 100 publications and 3 patents.